Journal of Medicinal Chemistry

ARTICLE

pubs.acs.org/jmc

Virtual Screening Targeting the Urokinase Receptor, Biochemical and Cell-Based Studies, Synthesis, Pharmacokinetic Characterization, and Effect on Breast Tumor Metastasis

Fang Wang,[†,‡] Jing Li,[†,‡] Anthony L. Sinn,[§,∥] W. Eric Knabe,[†] May Khanna,[†] Inha Jo,[†] Jayne M. Silver,[§,∥] Kyungsoo Oh,[⊥] Liwei Li,[†,#] George E. Sandusky,[▽] George W. Sledge, Jr.,[◆,●] Harikrishna Nakshatri,[†,●,¶] David R. Jones,[◆] Karen E. Pollok,[§,∥] and Samy O. Meroueh*[,†,●,⊥,#,+]

[†]Department of Biochemistry and Molecular Biology, [◆]Department of Medicine, [§]Herman B Wells Center for Pediatric Research, [∥]*In vivo* Therapeutics Core, [●]Indiana University Cancer Center, [#]Center for Computational Biology and Bioinformatics, [⊥]Department of Chemistry and Chemical Biology (IUPUI), [+]Stark Neurosciences Research Institute, [¶]Department of Surgery, and [▽]Department of Pathology and Laboratory Medicine, Indiana University School of Medicine, 535 Barnhill Drive, Indianapolis, Indiana 46202, United States

ABSTRACT:

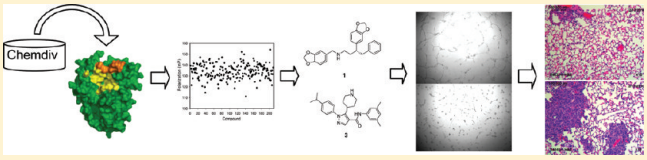

Virtual screening targeting the urokinase receptor (uPAR) led to (±)-3-(benzo[*d*][1,3]dioxol-5-yl)-*N*-(benzo[*d*][1,3]dioxol-5-ylmethyl)-4-phenylbutan-1-amine **1** (IPR-1) and *N*-(3,5-dimethylphenyl)-1-(4-isopropylphenyl)-5-(piperidin-4-yl)-1H-pyrazole-4-carboxamide **3** (IPR-69). Synthesis of an analogue of **1**, namely, **2** (IPR-9), and **3** led to breast MDA-MB-231 invasion, migration and adhesion assays with IC_{50} near 30 μM. Both compounds blocked angiogenesis with IC_{50} of 3 μM. Compounds **2** and **3** inhibited cell growth with IC_{50} of 6 and 18 μM and induced apoptosis. Biochemical assays revealed leadlike properties for **3**, but not **2**. Compound **3** administered orally reached peak concentration of nearly 40 μM with a half-life of about 2 h. In NOD-SCID mice inoculated with breast TMD-231 cells in their mammary fat pads, compound **3** showed a 20% reduction in tumor volumes and less extensive metastasis was observed for the treated mice. The suitable pharmacokinetic properties of **3** and the encouraging preliminary results in metastasis make it an ideal starting point for next generation compounds.

INTRODUCTION

When a primary tumor metastasizes, the prospects for survival become substantially worse, resulting in approximately 90% death in patients.[1] Metastasis occurs when cells from the primary tumor travel to distant sites and form new colonies. Cells escape from the primary tumors primarily through the circulatory system. These cells gain access to the vasculature as a result of multiple complex processes that involve invasion, migration, adhesion, and angiogenesis. A small number of cells that survive the voyage through the circulatory system arrive at new organ sites. Adhesion to and recognition of those sites in the endothelium are followed by re-entry through a process known as extravasation and result in the formation of a new tumor colony.

The urokinase receptor (uPAR) is a cell surface GPI-anchored protein that has been widely implicated with promoting metastasis. The receptor enhances pericellular proteolysis by serving as a docking site to the urokinase-type plasminogen activator (uPA), triggering a cascade of proteolytic events that include activation of plasminogen and matrix metalloproteinases (MMPs). The receptor also activates other cell signaling through lateral interactions with cell surface receptors that include integrins,[2] receptor tyrosine kinases (RTKs),[3,4] and G-protein coupled receptors (GPCRs). The dual roles of the urokinase system in promoting degradation of the ECM *and* signaling has implicated it with almost every step of tumor formation and progression, including tumorigenesis,[5] cell proliferation,[6,7] cell migration and adhesion,[8] angiogenesis,[9,10] and intravasation/extravasation.[11]

Toward the goal of discovering compounds that modulate interactions of uPAR and block invasion and metastasis in vivo, we used docking-based virtual screening to identify small molecules that bind to uPAR. We describe the successful outcome of this search, and the initial biological evaluations of the two most promising structures from this effort.

RESULTS

Structure-Based Virtual Screening by Docking Compounds to uPAR. Analysis of the three-dimensional structure

Received: June 16, 2011
Published: August 18, 2011

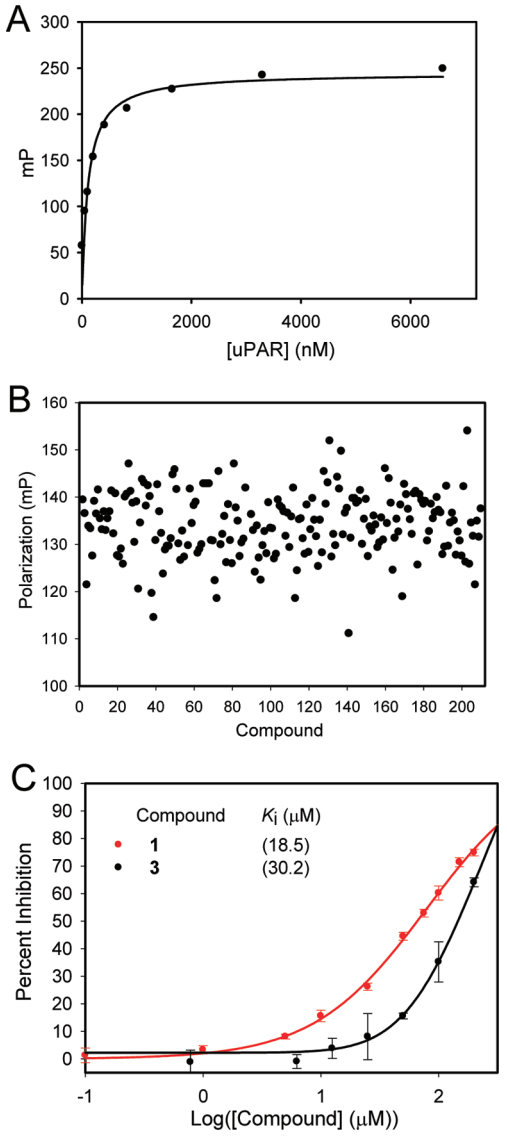

Figure 1. Biochemical evaluation of compounds. (A) Binding of fluorescent GFD (AE147-FAM) as a function of uPAR. Increasing concentrations of suPAR protein were titrated against the fluorescent GFD-FAM peptide. (B) Fluorescence polarization for the top compounds that emerged from the computational screening. (C) Abrogation of AE147-FAM binding to uPAR by **1** and **3** in a concentration-dependent manner.

of uPAR revealed a hydrophobic pocket that accommodates the growth factor domain (GFD) of its serine proteinase ligand uPA (PDB ID: 2FD6). A total of 300,000 compounds in the ChemDiv library were docked into the pocket using the computer program AutoDock4. The resulting complexes were scored with several scoring functions that include ChemScore,[12] Gold,[13] AutoDock,[14] and DOCK.[15] The top ranking 200 compounds for each scoring function were visualized, and clustered by chemical similarity. About 50 compounds were selected among the top compounds from each scoring function. A total of 210 compounds were acquired from ChemDiv for biochemical evaluation.

Biochemical Assessment of Compound Binding to uPAR. The design of a fluorescent probe was guided by the three-dimensional structure of uPAR in complex with peptide AE147.[16] As this peptide binds at the same site that is occupied

Scheme 1. Chemical Structure of Compounds That Showed Activity in the Fluorescence Polarization Assay

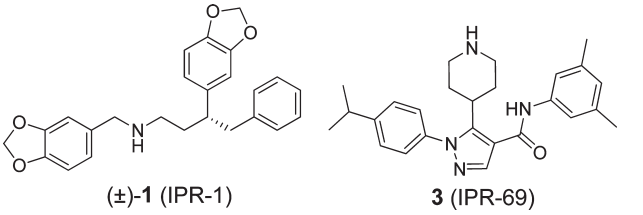

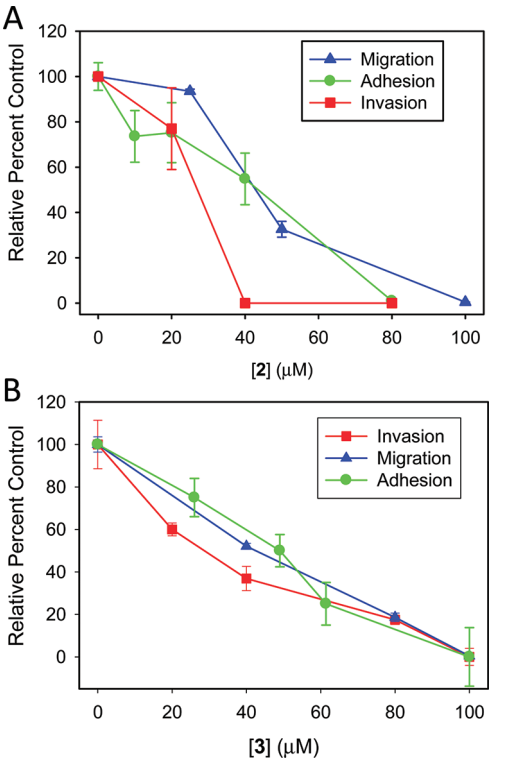

Figure 2. Effect on MDA-MB-231 metastasis. Concentration-dependent study of the effect of (A) **2** and (B) **3** on MDA-MB-231 invasion, migration and adhesion.

by the growth factor-like domain of uPA, it provides the basis for the development of a competition assay to assess binding to this site. Fluorescein was introduced to the N-terminus of AE147. The resulting peptide, AE147-FAM, binds to uPAR with high affinity with an estimated K_D of 120 nM, and shows similar potency to the EGF-like domain of uPA (Figure 1A).[16] All 210 compounds were screened at an initial concentration of 50 μM for displacement of AE147-FAM peptide. Eleven compounds gave polarization readings that were five times that of the standard deviation of the control peptide (Figure 1B). A secondary concentration-dependent study for these eleven compounds was performed. Among them, two compounds (Scheme 1) showed concentration-dependent inhibition (Figure 1C). The resulting inhibition curves were used to determine an inhibition constant, K_i, for each. The K_i value for (±)-3-(benzo[*d*][1,3]dioxol-5-yl)-*N*-(benzo[*d*][1,3]dioxol-5-ylmethyl)-4-phenylbutan-1-amine **1** (IPR-1) was 18 μM, while the K_i value for *N*-(3,5-dimethylphenyl)-1-(4-isopropylphenyl)-5-(piperidin-4-yl)-1H-pyrazole-4-carboxamide **3** (IPR-69) was 30 μM (Figure 1C).

dx.doi.org/10.1021/jm200782y |*J. Med. Chem.* 2011, 54, 7193–7205

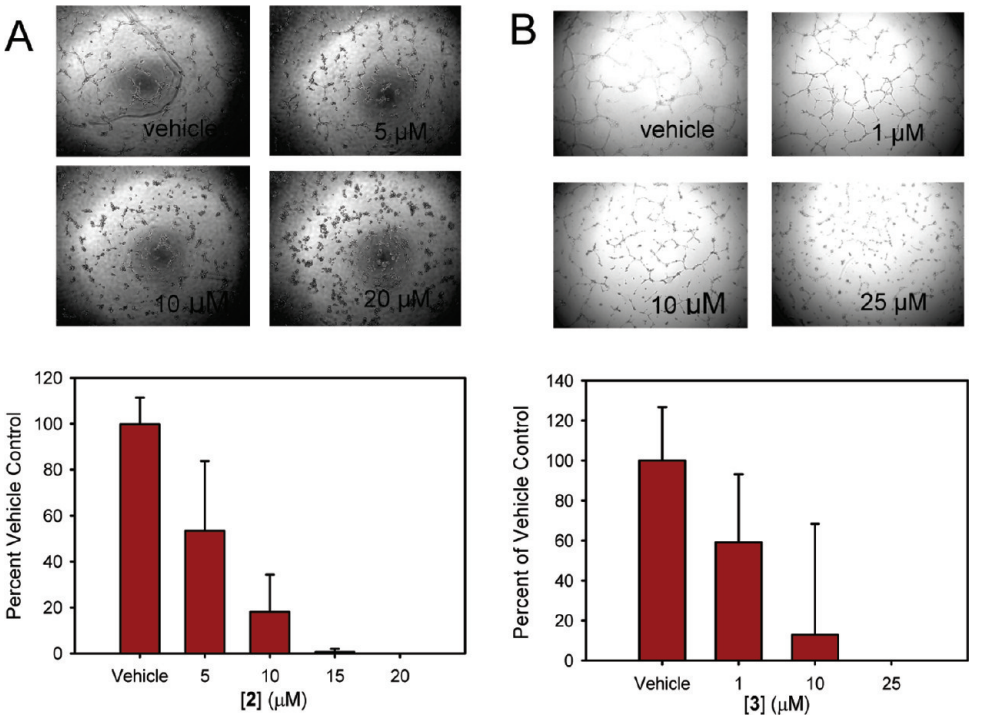

Figure 3. Effect of **2** and **3** tube formation in Matrigel by HUVEC cells. Snapshots depicting formation of capillary-like tubes of HUVEC after addition of DMSO (top left), and increasing concentration of (A) compound **2** and (B) compound **3**. Percentage of tube formation to the vehicle group was calculated for (A) compound **2** and (B) compound **3** in a concentration-dependent manner.

Cellular Assays To Probe Effect on Metastasis. We tested whether the two active compounds affected invasion, adhesion and migration in cell culture in a concentration-dependent study (Figure 2). For invasion, the Transwell (or Boyden) chamber assay was used.[17] The assay uses a chamber with two compartments that are separated by a microporous membrane known as Matrigel consisting of components of the ECM such as collagen, laminin and fibronectin.[17] Invasive tumor cells degrade the Matrigel and migrate through the membrane to the lower compartment. Instead of **1**, we tested a more soluble analogue, **2** (IPR-9). Compound **2** had an inhibition constant (20 μM) similar to that of **1**. Both **2** and **3** substantially impaired MDA-MB-231 invasion with IC_{50} of 30 μM for both compounds (Figure 2).

To assess whether compounds inhibit cell migration, the same Boyden chamber apparatus is used except that the porous membrane is not coated with the Matrigel layer. Compounds **2** and **3** significantly blocked migration of MDA-MB-231 across the membrane (Figure 2A). The IC_{50} values (43 μM for **2** and 40 μM for **3**) were somewhat larger than the values observed for invasion (Figure 2).

The effect of compounds on cell attachment (adhesion) to wells precoated with fibronectin was evaluated using an assay we have described previously.[18] Similar assays have evaluated extensively uPAR-mediated cell attachment to ECM components mediated by integrins.[19−21] Both **2** and **3** inhibited adhesion in a concentration-dependent manner with IC_{50} values of 45 μM (Figure 2).

Angiogenesis. The formation of new blood vessels from preexisting ones is known as angiogenesis, which is vital for tumor growth, invasion, and metastasis. The effect of **2** and **3** on angiogenesis was assessed in human umbilical vein endothelial cells (HUVEC) in a Matrigel-based tube formation assay.[22] The formation of these tubes is reminiscent of capillary formation in a tumor during angiogenesis. Both compounds inhibited tube formation in Matrigel in a concentration-dependent manner (Figures 3A and 3B). As illustrated from the images in Figures 3A and 3B, less tube formation is observed with increasing concentration of compound for both **2** and **3**. The extent of tube formation is quantified as shown by the histogram plots in Figures 3A and 3B and afforded an estimation of IC_{50}. Interestingly, both **2** and **3** showed greater potency in blocking angiogenesis by nearly an order of magnitude (IC_{50} = 3 μM) in comparison with invasion.

Effect on Cell Proliferation and Mechanism of Cell Killing. An MTT assay revealed that **2** and **3** inhibited cell proliferation with IC_{50} of 17 and 6 μM, respectively (Figures 4A and 4C). To gain insight into the mechanism by which these compounds are inhibiting growth, a flow cytometry analysis with annexin V−FITC and PI staining was performed. The level of apoptotic cells in MDA-MB-231 was assessed by the percentage of Annexin V-positive/PI-negative cells present after exposure of MDA-MB-231 cells to increasing concentration of **3** for 24 h (Figure 4D). At a concentration of 50 μM, **3** induced significant apoptosis as evidenced by a 51% and 21% increase in apoptotic cells (Annexin V positive/PI-negative) and necrotic cells (Annexin V-positive/PI-positive), respectively. A similar analysis for **2** indicated that the compound promoted cell death via both necrosis and apoptosis as illustrated in Figure 4B. At a concentration of 50 μM, 26% of cells were necrotic (Annexin V-positive/PI-positive), a 22% increase over control. 46% of cells were apoptotic (Annexin V-positive/PI-negative), compared with 4% of control.

Compounds 2 and 3 Block MMP-9 Activity in MDA-MB-231 Cells. To degrade collagen within the ECM, malignant cells unleash a series of extracellular proteases known as matrix metalloproteinases (MMPs). Inhibition of MMP activity with small molecules has been a cornerstone of efforts to develop

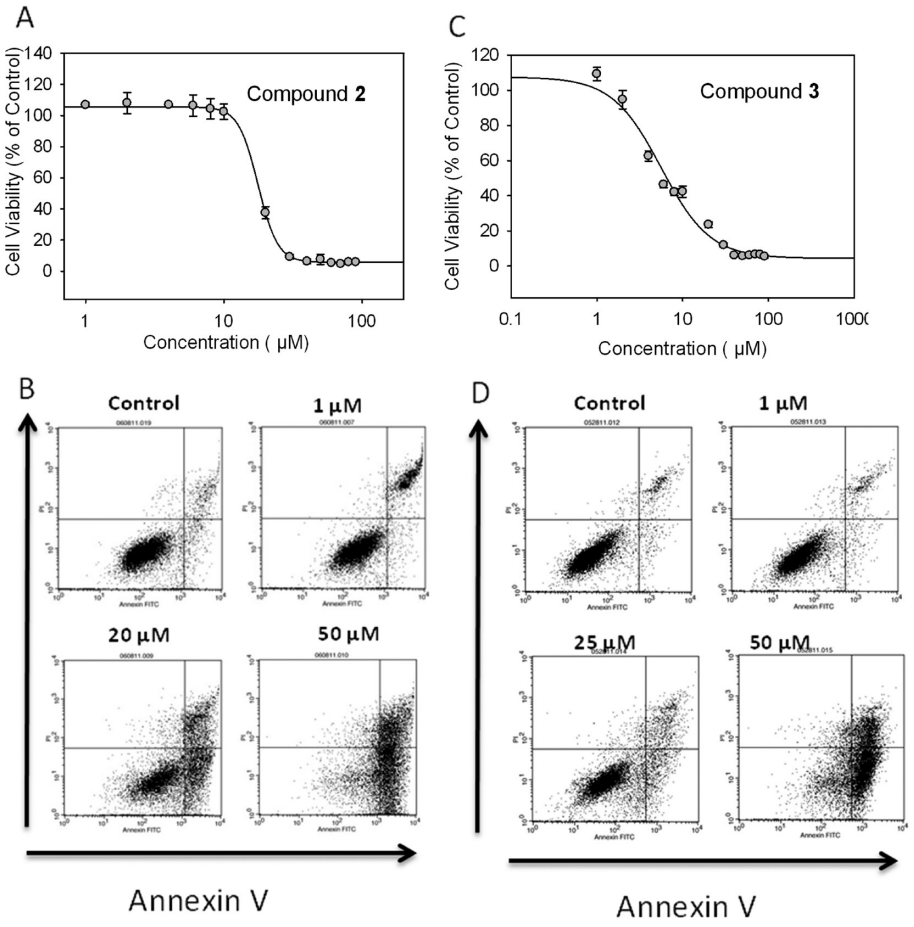

Figure 4. Inhibition of MDA-MB-231 proliferation and mechanism of cell killing. (A, C) MTT assay reveals that **2** and **3** inhibit MDA-MB-231 proliferation; (B, D) flow cytometry analysis using Annexin V−FITC and PI staining.

drugs that block tumor invasion and metastasis.[23] The gelatinases (MMP-2 and MMP-9) in particular have been strongly associated with invasion and metastasis. We assessed whether **2** and **3** impaired MMP-9 (gelatinase B) activity. When exposed to **2** and **3** at increasing concentration, MDA-MB-231 cells showed a concentration-dependent reduction in MMP-9 activity (Figures 5A and 5B). IC_{50} for inhibition of MMP-9 activity by **2** and **3** were estimated at 25 μM, which corresponded well with the IC_{50} for inhibition of invasion that were observed from the Boyden chamber study. At 50 μM, **3** nearly completely abrogated MMP-9 activity with 93% inhibition of its activity.

Cell Signaling. In light of the previously reported role of uPAR in signaling, the effect of **1**, **2**, and **3** on signaling was studied by Western blot analysis. Following exposure of the compounds at a concentration of 100 μM to MDA-MB-231 cells for 30 min, immunoblotting revealed significant impairment of MAPK phosphorylation by **1** and **2** (Figure 6A). Compound **3** also abrogated phosphorylation, but the effects were weaker than those of **2** and its parent compound (Figure 6A). A concentration-dependent study was subsequently carried out for **1** (Figure 6B). The results confirmed that the compound completely abrogated phosphorylation of MAPK, with an IC_{50} estimated at approximately 20 μM. The effect of the compound was also studied in two other signaling pathways including FAK and Src. FAK is constitutively associated with β-integrin subunits of integrin receptors. The compound did not show any significant effect on FAK phosphorylation compared with DMSO. Even less effect was observed on phosphorylation of Src, which is upstream of MAPK (Figure 6B). This suggests that **1** is unlikely to impair integrin signaling. The effect of the compounds on MAPK and the lack of effect on FAK and Src signaling suggest that the compounds are not promiscuous and their effects on metastasis can be attributed to the targeting of specific signaling pathways.

Synthesis of 2 and 3. The synthesis of N-1 substituted pyrazole **3** followed the route developed by scientists at Abbott Laboratories (Scheme 2). The pyrazole core was prepared by condensation of 1,3-dicarbonyl enol ethers with a variety of hydrazines. The yield was good to excellent in all cases.[24] Thus, commercially available N-Boc isonipecotic acid **4** was converted to known β-keto ester **6** through a simple two-step sequence (coupling of Meldrum's acid followed by ethanolysis).[25] Alternatively, condensation of the acid chloride of **6** with potassium ethyl malonate in the presence of a magnesium chloride-triethylamine base system also gave **7**.[26] With the requisite β-keto ester **7** in hand, the formation of pyrazole core was explored with commercially available 4-isopropyl phenylhydrazine. The amide bond formation followed by the removal of N-Boc gave the desired N-1 substituted pyrazole **3**.

The synthesis of a secondary benzyl amine, **2**, used 1,4-conjugate addition and reductive amination (Scheme 3). Thus, Knoevenagel condensation between commercially available

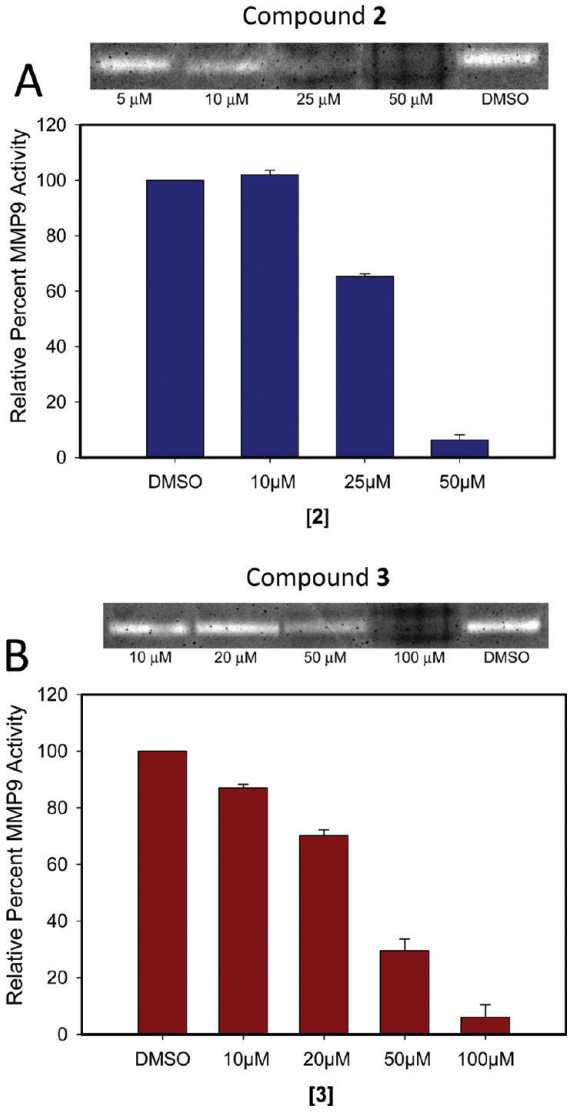

Figure 5. Effect on ECM degradation. Gelatin zymography analysis for MDA-MB-231 with increasing concentration of (A) compound **2** and (B) compound **3**.

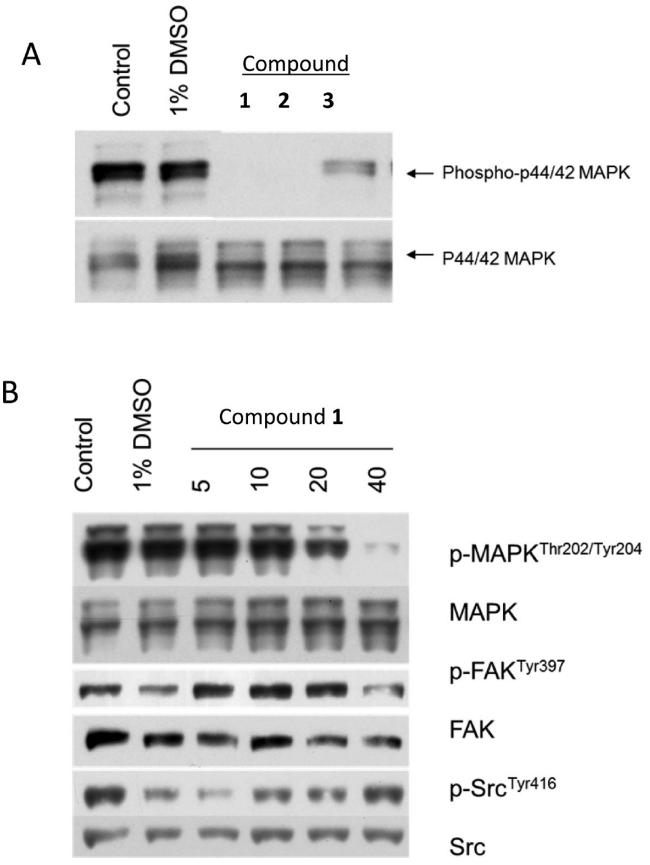

Figure 6. Cell signaling study. (A) MDA-MB-231 treated with 100 μM compound(s) for 30 min, then immunoblotted with phospho-p44/42 MAPK and p44/42 MAPK, respectively. (B) MDA-MB-231 treated with 5,10, 20, and 40 μM compound(s) for 30 min, then immunoblotted with phospho-p44/42 MAPK (Thr202/Tyr204), p44/42 MAPK; phospho-FAK (Tyr397), FAK; phospho-Src family (Tyr416), Src, respectively.

phenylacetaldehyde and diethyl malonate using a catalytic amount of piperidine and acetic acid in refluxing toluene gave **11**, which was then subjected to the conjugate addition conditions developed by Bosch, where excess CuCl promoted an efficient conjugate addition of Grignard reagents. With the desired Michael adduct **12** to aldehyde **15** was achieved by a sequence of conventional functional group manipulation: hydrolysis, decarboxylation, reduction, and oxidation. The reductive amination between aldehyde **15** and commercially available 4-(dimethylamino)benzylamine dihydrochloride gave the desired secondary amine **2** as a racemate.

In Vitro Studies for Insights into PK Properties of 3. Inhibition of the hERG channel is undesirable. Checking for hERG blockage is an integral step in the drug discovery cycle. We employ a method that is well-suited for high-throughput measurements based on fluorescence polarization (FP) as implemented in the Predictor Assay by Invitrogen (Carslbad, CA). This assay is based on the principle that a fluorescent tracer upon binding to the hERG channel will induce an increase in the FP signal that will diminish when an inhibitor displaces the interaction between the tracer and the hERG channel. Data generated with this assay was shown to correlate well with patch-clamp assay measurements.[27] We performed FP measurements for **2** and **3** using an EnVision (PerkinElmer) plate reader at an excitation of 540 nm and emission at 573 nm. As shown in Figure 7A, **1** and its derivative blocked the channel at all three concentrations considered (1, 10, and 25 μM). In fact, these two compounds showed even greater potency than the well-known channel blocker E-4031.[28] Compound **3**, on the other hand, exhibited lower levels of hERG blockage. At the highest concentration of 25 μM, which is near its biological activity in tumor cells, 60% blockage is detected.

Another source of toxicity for drugs is cytochrome P450 (CYP) inhibition. CYPs detoxify harmful compounds and catalyze key reactions in the formation of endogenous compounds such as hormones and steroids.[29] Studies have shown that 90% of drugs are metabolized by at least one of the seven known CYP isoforms (CYP-1A2, 2C9, 2C18, 2C19, 2D6, 2E1 and 3A4). We assayed CYP metabolism using a fluorescence-based assay,[30] recently implemented by Invitrogen (Carlbad, CA). Compounds **1**, **2** and **3** were evaluated for inhibition of CYP2C9. As a positive control, the CYP2C9 inhibitor sulfaphenazole inhibited the metabolism of the fluorescent substrate by

dx.doi.org/10.1021/jm200782y |J. Med. Chem. 2011, 54, 7193–7205

Scheme 2[a]

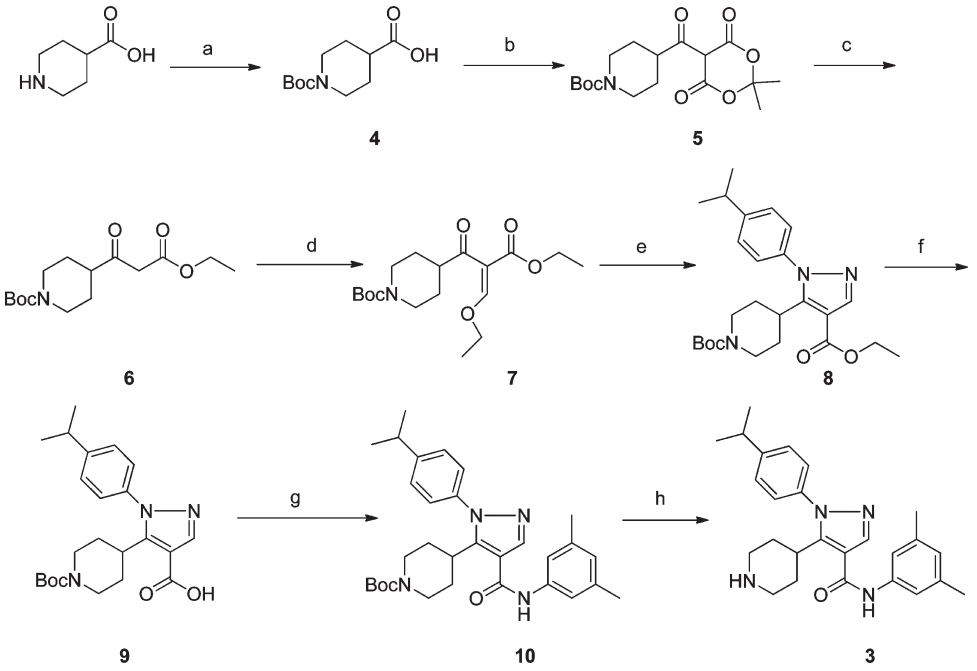

[a] Reagents and conditions: (a) K_2CO_3, di-*tert*-butyl dicarbonate, THF:H_2O, 0 °C; (b) DMAP, DCC, 2,2-dimethyl-1,3-dioxane-4,6-dione, DCM, 0 °C; (c) ethanol, reflux; (d) triethylorthoformate, acetic anhydride, reflux; (e) ethanol, 4-isopropyl phenyl hydrazine, reflux; (f) 2.0 M NaOH (aq), ethanol, 70 °C; (g) DMAP, DCC, 3,5-dimethylaniline, DCM, 0 °C; (h) trifluoroacetic acid:DCM, 0 °C.

~69% at 5 μM (Figure 7B). Little inhibition was observed for **1** and **2** at 1 μM, but more significant inhibition at concentrations that are comparable to their biological activity. At 25 μM, these compounds inhibit the enzyme by nearly 80%, comparable to the levels seen for sulfaphenazole, suggesting potential toxicity in vivo. Compound **3**, on the other hand revealed little inhibition of CYP2C9 (Figure 7B). Even at 25 μM, only 20% inhibition is detected, comparable to what we have observed for FDA-approved drugs.[31]

Finally, we assessed DNA binding by these three compounds. DNA binding is often a reflection of nonspecificity, which can lead to adverse side effects. We employ a well-established fluorescent intercalator displacement assay[32] that measures displacement of ethidium bromide, a known intercalator of DNA. In this assay, ethidium bromide (EB) bound to the salmon sperm DNA. DNA binding was not strongly affected at the three concentrations of **1**, **2**, and **3** that were tested. A 30% displacement of ethidium bromide was observed for **1** and **2**, while **3** showed less than 10% displacement at 25 μM (Figure 7C).

In Vivo PK Study of 3. Compound **3** was administered to mice via a single oral gavage of 100 mg/kg using a formulation of 0.5% (w/v) of methylcellulose and 0.1% of Tween 20. Blood (20 μL) was taken from the mice at their tails at time intervals of 1, 2, 4, 12, 24, 36, and 48 h (two time points from each of the 22 mice[33]) post injection. Blood plasma samples were prepared by centrifugation for quantification and HPLC−MS/MS analysis. Compound **3** was quantified as shown in Figure 7D, and the resulting PK parameters are provided in Figure 7E. Compound **3** was detected in plasma at a maximum level of 40 μM at ~5 h after administration. A half-life was estimated at 2 h. These parameters suggest that **3** possesses suitable druglike properties in vivo and sets the stage for further optimization of the potency of the compound.

Role of 3 in MDA-MB-231 Metastasis in Vivo. The effect of **3** in blocking metastasis and growth in cell culture, along with its favorable in vivo pharmacokinetic properties prompted evaluation of its effect on metastasis in vivo. TMD-231 cells were inoculated into the mammary fat pad of female NOD/SCID mice. Dosing was initiated at day 18 post implantation. Animals were randomized and treated with vehicle or with **3** by daily oral gavage at a dose of 150 mg/kg (n = 11). Tumor volumes were determined by caliper measurements on a twice weekly basis, and calculated according to the formula $(\alpha^2 \times \beta)/2$, where α is the shorter and β is the longer of the two dimensions. Tumor volumes were determined by caliper measurements on a weekly basis. The study was conducted over a period of 68 days. The primary tumor in both control and treated mice grew substantially over the course of the study. Tumor volumes reached nearly 965 mm^3 for untreated mice. For treated mice, tumor volumes reached an average of 779 mm^3 at the end of the study, a 20% reduction (Figure 8A).

Over the course of the study, several mice were sacrificed to determine whether breast tumor cells had metastasized to the lungs. At the end of the study, control and experimental animals were sacrificed and organs (lungs) were removed and evaluated for the presence of tumors. The number and size of metastasis in two to five fields per sample were calculated. A score of 4+ was given to a sample with highest metastasis index, and relative metastasis in other samples was calculated (i.e., 1+, 2+, 3+) by a sample-blinded pathologist. In the untreated mice, 9 out of 11 mice had metastatic foci in the lungs (score = 0). In contrast, only 3 out of 11 treated mice showed signs of metastatic lesions. The extent of metastasis in treated versus untreated was also different.

dx.doi.org/10.1021/jm200782y |*J. Med. Chem.* 2011, 54, 7193–7205

Scheme 3[a]

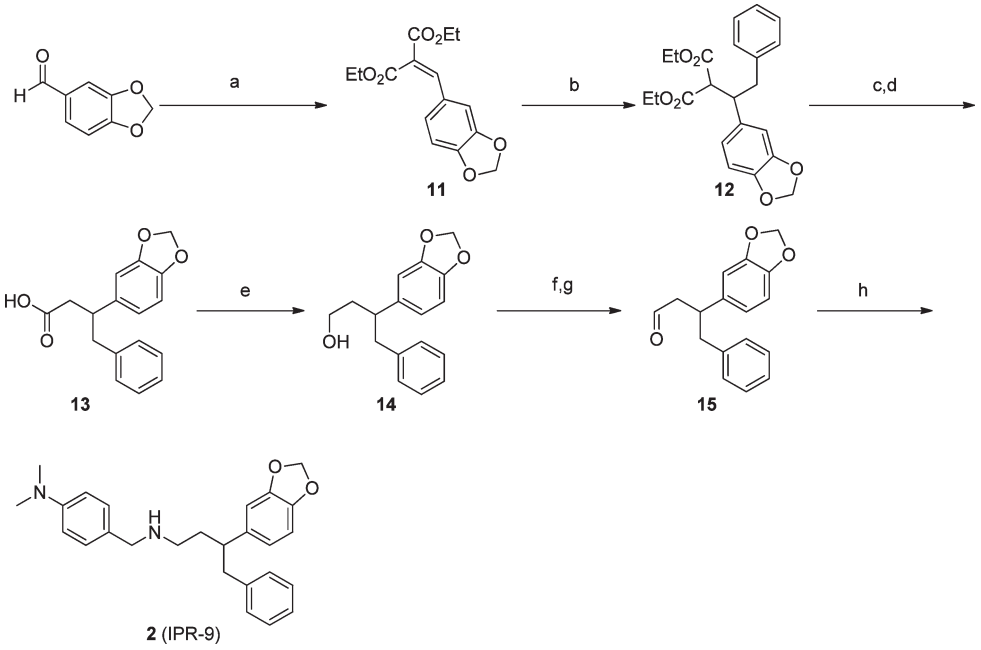

[a] Reagents and conditions: (a) cat. piperidine/AcOH toluene, reflux, diethyl malonate; (b) BnMgCl, CuCl, −78 °C to rt ; (c) 10% KOH MeOH:H_2O (1:1) rt; (d) *p*-xylene, reflux; (e) $LiAlH_4$, THF 0 °C to rt; (f) Et_3N, DMSO, SO_3Py, DCM, 0 °C; (g) 4-(aminomethyl)-*N*,*N*-dimethylaniline hydrochloride, (h) $Na(AcO)_3BH$, THF, rt.

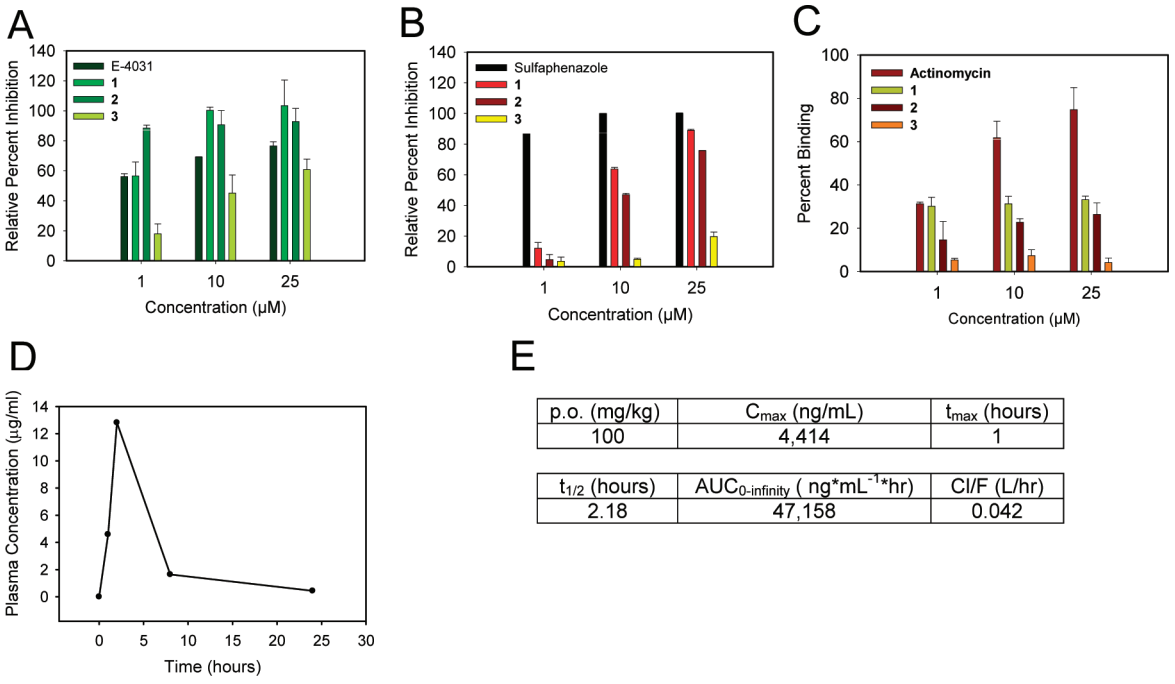

E

p.o. (mg/kg)	C_{max} (ng/mL)	t_{max} (hours)
100	4,414	1

$t_{1/2}$ (hours)	$AUC_{0\text{-infinity}}$ (ng*mL^{-1}*hr)	Cl/F (L/hr)
2.18	47,158	0.042

Figure 7. In vitro and in vivo PK parameters. (A) Percent blockage of hERG K+. E-4031 is used as control. (B) Percent inhibition of CYP2C9 isozyme. Sulfaphenazole is used as control. (C) DNA binding of compounds using fluorescence emission (excitation, 530 nm, and emission, 615 nm) of calf thymus DNA bound to ethidium bromide (DNA-EB). Actinomycin D (ActD), a known DNA intercalator, is used as positive control. (D) PK analysis of **3** in female NOD/SCID mice (n = 1 per time point) dosed by oral gavage as a mixture of 100 mg/kg in 0.5% hydroxy-methyl-propyl-cellulose. (E) In vivo PK parameters.

Fewer of the treated mice developed substantial metastasis with a score >2. For example, 5 of the untreated mice exhibited increased metastatic lesions (score >2), compared with only 3 of the treated mice (Figure 8B). Finally, more of the untreated

dx.doi.org/10.1021/jm200782y |*J. Med. Chem.* 2011, 54, 7193–7205

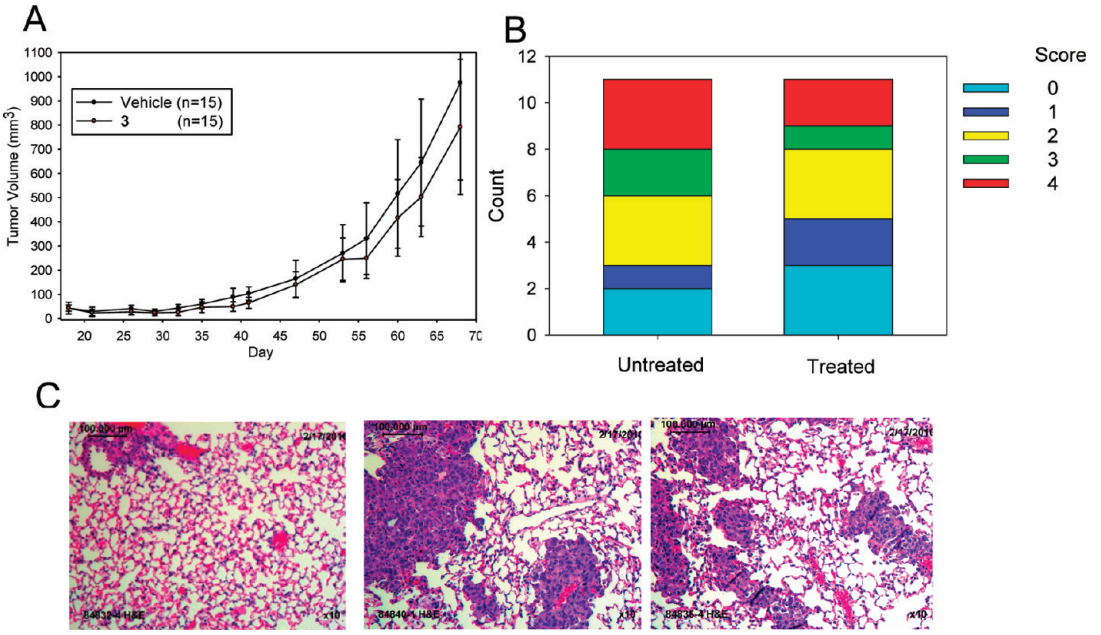

Figure 8. Effect of **3** on MDA-MB-231 tumor growth. (A) MDA-MB-231 cells were inoculated in the mammary fat pads of female NOD/SCID mice. Once the tumor volume reached 30 to 50 mm^3, animals were randomized and treated with vehicle alone as control or 150 mg/kg of compound **3** three times a week for 10 weeks by oral gavage. Tumor volumes were determined by caliper measurements obtained weekly as described in Materials and Methods. (B) A semiquantitative scoring system was used for the estimation of TMA scoring. Briefly, percentage of staining was categorized as "0" if there was no nuclear/cytoplasmic expression, "1" for up to 10% positive tumor nuclei/cells, "2" for 11−20% and until a maximum score of "10". Intensity was scored as "1+," "2+," and "3+" for weak, moderate and strong staining respectively. (C) H&E staining images that illustrate metastasis in the lungs.

mice developed metastatic lesions with a score of 4 or greater (Figure 8B). An illustration of the extent of metastasis to the lungs is shown in Figure 8C with H&E staining images for control and treated mice.

DISCUSSION

Throughout the metastatic process, malignant cells unleash a series of proteases that systematically degrade components of the ECM, not only to eventually gain access to the vasculature (extravasation), but also following attachment to new sites to create new colonies (intravasation). When a distant colony is established during metastasis, a constant supply of nutrients is needed to sustain the level of growth required for the tumor to establish itself and begin the process of metastasis anew. This process, known as angiogenesis, also requires the contribution of proteases. uPAR plays an important role in these processes, not only by anchoring proteases at the cell surface, but also by engaging other receptors at the cell surface. Using virtual screening, a chemical library of nearly 300,000 molecules was screened for compounds that bind to uPAR. We identified active compounds by computation that were then shown experimentally to bind directly to uPAR.

Cellular studies revealed that two of these compounds, **2** and **3**, blocked invasion, migration, and adhesion of MDA-MB-231 breast cancer cells in cell culture. Both these compounds also impaired angiogenesis in tube formation assays using HUVECs with an IC_{50} nearly an order of magnitude better (IC_{50} = 3 μM) than those observed in the invasion studies. Gel zymography analysis revealed that the compounds impaired MMP-9 activity in a concentration-dependent manner with IC_{50} that are comparable to those measured in the invasion studies. This was encouraging, since previous studies have shown that uPA promotes degradation of the ECM through activation of MMP-9 activity. Compounds **2** and **3** inhibited MDA-MB-231 proliferation (IC_{50} = 17 and 6 μM, respectively), and subsequent flow cytometry analysis with annexin V staining revealed that both induced apoptosis, while **2** also caused significant necrosis. Signaling studies showed that both compounds impaired MAPK phosphorylation, but **1** was more potent. Compound **1** did not show any effect on FAK and Src signaling, suggesting that these compounds are unlikely affecting integrin-mediated signaling. Past studies have shown that uPAR can enhance signaling through integrins. The lack of effect of **1** on integrin signaling suggests that the uPA binding site is unlikely contributing to integrin signaling and that other sites on the receptor, such as the vitronectin binding site, are responsible for interaction with integrins.

A series of biochemical assays that included DNA binding, cytochrome P450 inhibition, and hERG K+ channel blockage provided insight into the druglikeness properties of the compounds. Compound **3** exhibited the most favorable properties, showing no DNA binding, little inhibition of CYP2C9, and lower levels of hERG channel blockage. In contrast, **1** and its derivative, **2**, showed significant impairment of CYP2C9 activity and even greater hERG K+ channel blockage than the well-known channel blocker E-4031. These results led us to focus on **3** and assess its PK properties in vivo. The compound was orally bioavailable, reaching concentrations of up to 40 μM with half-life of approximately 2 h when administered. The compound was well tolerated at doses as high as 150 mg/kg. These promising results prompted efficacy studies to evaluate its antimetastatic effect in vivo using a triple-negative TMD-231 (MDA-MB-231 variant) implanted in breast mammary fat pads. It was interesting that treated mice developed primary tumors that were on average

20% lower in size than untreated mice. In addition, the treated mice showed less metastasis to the lungs when compared with the untreated group.

It is likely that some of the anticancer effects of **3** are enhanced by off-targets. Given the effects of **3** on invasion and angiogenesis, we have explored the possibility that the compound may bind and inhibit MMP-9 or the vascular endothelial factor receptor (VEGFR), key mediators of invasion and angiogenesis. The compound was docked to the active site of MMP-9 and VEGFR2 (PDB codes 1GKC and 3EWH, respectively) using the Vina docking program. The resulting complexes along with the complex of **3** bound to uPAR were scored with the X-score scoring function, which we have recently shown to perform best in rank-ordering complexes. The resulting scores were −9.2, −9.7, and −9.7 for uPAR, MMP-9 and VEGFR2, respectively. While conclusive evidence will have to be obtained from biochemical studies, the similarity of these scores suggests that either MMP-9 or VEGFR2 may also be targets of the compound.

Cancer is a systems biology disease that involves multiple signaling pathways. Compounds with polypharmacology that target more than one pathway may lead to cancer therapeutics with greater efficacy. Therefore, off-targets that enhance the anticancer properties of a compound may be welcome, as long as they do not cause undue toxicity. Compound **3** seems to be well tolerated even at concentrations of 150 mg/kg and caused little toxicity, suggesting that off-targets are unlikely causing toxicity. The promising PK properties and the encouraging effects on tumor growth and metastasis in vivo suggest **3** as an excellent platform upon which to develop derivatives with greater efficacy in vivo.

MATERIALS AND METHODS

Fluorescence Polarization Assay. Our fluorescence polarization assay used fluorescent AE147-FAM peptide. uPAR was titrated against the fluorescent AE147-FAM peptide, and data were fit to a sigmoidal dose-dependent curve as the FP value increases to determine the K_d of binding using Sigmaplot (Systat Software Inc., CA). Inhibitor screens were carried out in triplicate using 500 nM uPAR, 100 nM AE147-FAM, and inhibitor concentrations ranging from 0.78 μM to 100 μM in 50 μL volumes in a black BD Falcon 384-well microplate. The compounds were serially diluted in DMSO and then diluted in 0.01% Triton X-100 in 1× PBS buffer ensuring a final concentration of 2% DMSO (a concentration that did not affect peptide binding to uPAR). Polarized fluorescence intensities were measured immediately following addition of inhibitors to the protein−peptide mix at room temperature on an EnVision Multilabel Plate Reader (PerkinElmer) with excitation and emission wavelengths of 485 and 530 nm, respectively.

Proliferation Assay. The procedure consisted of culturing cells at 37 °C in 10% FBS-DMEM medium containing various amounts of compound. 20 mM compound stock in 100% DMSO was 1:50 diluted in medium, filtered, and serially diluted in a 96-well plate. Then seeded cells were incubated for 3 days. Viable cells were quantified by MTT assay at absorbance of 570 and 630 nm.

Invasion and Migration Assays. This was performed using BD BioCoat Matrigel Invasion Chamber (cat. 354480, BD Biosciences, Bedford, MA). The undersurfaces of the inserts were coated with 30 μg/mL of fibronectin (Sigma, F2006) in PBS at 4 °C overnight. The inserts were washed with PBS once. 0.5 mL of serum-free medium was separately added to the upper and lower chambers to equilibrate the Matrigel invasion chambers at 37 °C, 5% CO_2 for 2 h. After starvation with serum-free DMEM for 4 h, subconfluent MDA-MB-231 cells were trypsinized and resuspended in 0.1% FBS DMEM. 5 $\times 10^4$ cells in 500 μL of 0.1% FBS DMEM containing various compounds or 1.0% DMSO (as control) were added to the upper chambers. 500 μL of 10% FBS DMEM containing the same concentration of the same compound or DMSO were added to the lower chambers. We incubated the invasion chambers for 3 h at 37 °C, 5% CO_2. Noninvaded cells were removed from the upper chamber with a cotton swab. The invaded cells were fixed with 100% methanol and then stained with Hematoxylin Stain Harris Modified Method (Fisher, SH30-500D). We washed the filters with water 3 times. Filters were air-dried, and the invaded cells were counted in ten randomly selected microscopic fields (×200 magnification). The experiment was performed in triplicate per group and shown by mean ± SE.

Gelatin Zymography. MDA-MB-231 cells were treated with different concentrations of uPAR compounds in serum free medium for 24 h, the conditioned medium was collected and concentrated by Amicon Ultra centrifugal filter units (Millipore, #UFC500324), and proteins were normalized and electrophoresed on sodium dodecyl sulfate (SDS)−polyacrylamide gels (10%) containing 1 mg/mL gelatin. After electrophoresis, the gel was washed twice in 50 mM Tris-HCl (pH 7.6) containing 5 mM $CaCl_2$ and 2.5% Triton X-100 for 30 min at room temperature and incubated in buffer that contained 50 mM Tris-HCl (pH 7.6), 200 mM NaCl, 10 mM $CaCl_2$ at 37 °C for 36 h. Then, the gels were stained with 0.05% Coomassie brilliant blue (CBB) and destained with 30% methanol in 10% acetic acid. Areas of gelatinolytic degradation appeared as transparent bands on the blue stained background of the gel. Data were quantified using Image J.

Adhesion Assay. Quantitative cell adhesion assays were carried out in non-tissue culture treated 96-well microtiter plates (Evergreen Scientific, Los Angeles, CA) which were coated with 15 μg/mL fibronectin (Sigma) for 1 h at room temperature. Fibronectin coated and uncoated control wells were blocked for 1 h with 3% heat-denatured bovine serum albumin (BSA) at 37 °C. Cells were split 1 day prior to the experiment to achieve a subconfluent culture. Briefly, MDA-MB-231 cells were collected with trypsin, quenched with soybean trypsin inhibitor (Calbiochem), and washed twice with serum-free medium, and 2 × 10^4 cells in 100 μL of serum-free medium containing various compounds were added to each well, quadruplicate per group and incubated for 90 min at 37 °C. The wells were washed, and the number of adherent cells was quantified by crystal violet staining at 570 nm.[34,35] The results were shown by means ± SE.

Angiogenesis Assay. Matrigel assays were performed as previously described with minor modifications.[36] Early passage (2−3) cord blood-derived endothelial cells were seeded onto 96-well tissue culture plates coated with 40 μL of Matrigel (BD Biosciences) at a cell density of 7500 cells per well. Cells were observed every 2 h by visual microscopy with an inverted microscope at 40× magnification for capillary-like formation. The percentage of the tube formation to the vehicle control group was calculated for each compound treated group.

Cloning, Expression and Purification of uPAR. We have successfully cloned, expressed and purified uPAR. From 1 L of culture, we express nearly 12 mg of protein, which will be sufficient to conduct the experiments that we propose in this study. Briefly, a truncated, soluble form of human uPAR (suPAR, amino acids 1−283) was expressed in stably transfected *Drosophila* S2 cells using the *Drosophila* Expression System (Invitrogen). suPAR was obtained by a two-step purification process. The conditioned culture medium was filtered (0.45 μm) and loaded onto a DEAE Sephadex column equilibrated with 20 mM Tris (pH 7.4). The protein was eluted with a gradient of 0−1 M NaCl in 20 mM Tris (pH 7.4). suPAR containing fractions were then pooled, concentrated, and filtered prior to RP-HPLC using a semipreparative (10 × 25 cm) C8 column. A 1 mL aliquot of the concentrated protein was loaded onto the column at initial gradient conditions of 95% eluent A and 5% eluent B, where eluent A was 0.1%

TFA/100% H_2O and eluent B was 70:30 acetonitrile/0.00085 MeCN/H_2O/TFA. The protein elutes using a gradient of 5% eluent A to 95% eluent B over 46 min at a flow rate of 4 mL/min. Under these conditions, the protein eluted as a single sharp peak (t_R = 29 min). SDS−PAGE analysis of the uPAR containing fractions showed a single band at the expected mass of 60 kDa. Surface plasmon resonance confirmed that the purified uPAR was capable of binding to uPA. The identity of the 60 kDa band was established by immunoblot (not shown).

Apoptosis Assay. MDA-MB-231 cells were cultured in DMEM medium supplemented with 10% FBS, 100 IU/mL penicillin and 50 μg/mL streptomycin in a humidified atmosphere containing 5% CO_2 at 37 °C and grew to 80−90% confluence in 60 mm plates. Then they were treated with various amounts of compounds or 1% DMSO (as control) for different time points. The cells were washed with 1× PBS twice and detached by using cellstripper (Mediatech Inc., VA), washed twice with cold 1× PBS and resuspended in 1× binding buffer (Cat. PNN1001, Invitrogen Corporation, Camarillo, CA) at a concentration of 1 × 10^6 cells/mL. 100 μL of the solution (1 × 10^5 cells) was transferred to a 5 mL culture tube. 5 μL of recombinant human annexin V−FITC conjugate (Cat. ANNEXINV01, Invitrogen) and 5 μL of propidium iodide solution (Cat. P4864, Sigma-Aldrich, St. Louis, MO) were added. The cells were gently vortexed and incubated for 15 min at room temperature (25 °C) in the dark. 400 μL of 1× binding buffer was added to each tube. Analysis was by flow cytometry (FACScan).

Immunoblots. MDA-MB-231 cells were treated with 100 μM of compound(s) and 1% DMSO for 30 min. Harvested cells in RIPA buffer were supplemented with protease inhibitors and phosphatase inhibitors. Under nonreducing conditions equal amounts of protein were loaded per lane and separated in 4−12% NuPAGE gel (Invitrogen) at 200 V for 60 min, then transferred to nitrocellulose membrane at 30 V for one hour using XCell II blot module. For immunoblotting, the first antibody was Phosph-p44/42 MAPK (Thr202/Tyr204) (D13.14.4E) rabbit mAb (#4370, Cell Signaling Technology, Inc., Danvers, MA) 1:2000 or P44/42 MAP Kinase (137F5) rabbit mAb (#4695, Cell Signaling Technology, Inc., Danvers, MA) 1:500 in 5% nonfat milk-TBST at 4 °C overnight. Secondary antibody consisted of goat anti-rabbit IgG HRP 1:3000 in 5% nonfat milk-TBST at room for 1 h. The protein bands were visualized using Immobilon Western Chemiluminescent HRP Substrate (WBKLS0100, Millipore, Billerica, MA).

Fibronectin (Sigma, F2006) 30 μg/mL was coated in 6-well plates overnight. MDA-MB-231 cells were serum-starved for 4 h, then seeded in FN coated 6-well plates and treated with 5,10, 20, and 40 μM compound(s) and 1% DMSO for 30 min; cells were lysed in RIPA buffer supplemented with protease inhibitors and phosphatase inhibitors. Then immunoblotting with phospho-p44/42 MAPK (Thr202/Tyr204), p44/42 MAPK; phospho-FAK (Tyr397), FAK; and phospho-Src family (Tyr416), Src, was carried out respectively.

Synthesis. All chemicals were purchased from either Aldrich or Acros and used as received. Column chromatography was carried out with silica gel (25−63 μm). Mass spectra were measured on an Agilent 6520 Accurate Mass Q-TOF instrument. ^{1}H NMR spectra were recorded in $CDCl_3$ or methanol-d_4 on a Bruker 500 MHz spectrometer. Chemical shifts are reported using residual $CHCl_3$ or MeOH as internal references. All compounds that were evaluated in biological assays had >95% purity using HPLC.

*1-(tert-Butoxycarbonyl)piperidine-4-carboxylic Acid (**4**).* To a stirred solution of isonipecotic acid (77.4 mmol, 10.0 g) and potassium carbonate (154.8 mmol, 21.4 g) in water (150 mL) at 0 °C was added dropwise a solution of di-*tert*-butyl dicarbonate (77.4 mmol, 16.9 g) in THF (150 mL). The reaction mixture was gradually warmed to rt and stirred overnight. The solvents were evaporated, and the residue was dissolved in DCM. The DCM layer was washed with 1 N HCl (3 × 100 mL) and then water, dried over sodium sulfate, and concentrated in vacuo to give pure **4** (13.03 g, 75%) as a white powder: ^{1}H NMR (500 MHz, $CDCl_3$) δ 4.02 (br s, 2H), 2.85 (t, *J* = 11.5 Hz, 2H), 2.49 (m, 1H), 1.90 (d, *J* = 11.5 Hz, 2 H), 1.65 (m, 2H), 1.45 (s, 9H); ^{13}C NMR (125 MHz, $CDCl_3$) δ 180.1, 154.7, 79.7, 40.7, 28.3, 27.6; MS calcd for $C_{11}H_{18}NO_4$ $(M - H)^-$ 228.1241, found 228.1240.

*tert-Butyl 4-(2,2-Dimethyl-4,6-dioxo-1,3-dioxane-5-carbonyl)piperidine-1-carboxylate (**5**).* To a stirred solution of **4** (56.8 mmol, 13.03 g) and DMAP (5.68 mmol, 694 mg) in DCM (10 mL) at 0 °C were added DCC (62.5 mmol, 12.9 g) and 2,2-dimethyl-1,3-dioxane-4,6-dione (62.5 mmol, 9.00 g) sequentially. The reaction mixture was gradually warmed to rt and stirred overnight. The reaction mixture was filtered and washed with DCM. The resultant orange solution was concentrated in vacuo. Product was used directly without isolation.

*tert-Butyl 4-(3-Ethoxy-3-oxopropanoyl)piperidine-1-carboxylate (**6**).* To **5** was added absolute ethanol (200 mL), and the solution was refluxed for 48 h. The solution was concentrated in vacuo and purified by flash chromatography (DCM) to give **3** as a reddish oil (14.36 g, 85%): ^{1}H NMR (500 MHz, $CDCl_3$) δ 12.09 (s, 0.14H, enol OH), 4.89 (s, 0.14H, enol C−H), 4.13 (q, *J* = 7 Hz, 2H), 4.10−3.96 (m, 2H), 3.42 (s, 2H), 2.81−2.67 (m, 2H), 2.62−2.52 (m, 1H), 1.85−1.71 (m, 2H), 1.55−1.43 (m, 2H), 1.39 (s, 9H), 1.21 (t, *J* = 7 Hz, 3H); ^{13}C NMR (125 MHz, $CDCl_3$) δ 204.0, 180.2 (enol), 172.7 (enol), 167.0, 154.4, 87.52, 79.51, 61.3, 48.5, 47.1, 28.2, 27.1, 13.9; R_f = 0.2 (DCM); HRMS calcd for $C_{15}H_{26}NO_5$ $(M + H)^+$ 300.1805, found 300.1808.

*(E,Z)-tert-Butyl 4-(3-Ethoxy-2-(ethoxycarbonyl)acryloyl)piperidine-1-carboxylate (**7**).* Under argon, **6** (47.9 mmol, 14.36 g), triethyl orthoformate (143.7 mmol, 24 mL), and acetic anhydride (95.8, 9 mL) were mixed and refluxed at 100 °C for 48 h. Low-boiling impurities were evaporated off, and the crude product was purified by flash chromatography (DCM) to give **7**, as a yellow-colored oil (14.92 g, 88%); R_f = 0.22 (1% MeOH/DCM); ^{1}H NMR (500 MHz, $CDCl_3$) δ 7.59 (s, 0.54 H, minor), 7.52 (s, 1H, major), 4.24 (q, *J* = 7.1 Hz, 2H), 4.21−4.09 (m, 7H), 4.08−3.92 (m, 4H), 3.09−3.01 (m, 0.58H, minor), 2.95−2.87 (m, 1H, major), 2.83−2.67 (m, 4H), 1.85−1.67 (m, 4 H), 1.58−1.47 (m, 4H), 1.41 (s, 19H), 1.37−1.26 (m, 9H), 1.23 (t, *J* = 7.1 Hz, 6H); ^{13}C NMR (125 MHz, $CDCl_3$) δ major isomer, 201.7, 165.7, 165.3, 162.3, 154.61, 112.6, 79.3. 72.2, 60.5, 48.0, 45.4, 28.3, 27.2, 15.2, 14.2; minor isomer, 199.6, 165.2, 154.59, 112.9, 72.7, 60.7, 28.0, 15.1, 14.1; MS calcd for $C_{18}H_{30}NO_6$ $(M + H)^+$ 356.2068, found 356.2067.

*tert-Butyl 4-(4-(Ethoxycarbonyl)-1-(4-isopropylphenyl)-1H-pyrazol-5-yl)piperidine-1-carboxylate (**8**).* Free hydrazine was prepared from HCl salt by washing with saturated sodium bicarbonate solution and extracting with DCM. DCM was removed in vacuo. To a stirred solution of free 4-isopropyl phenyl hydrazine (21.7 mmol, 3.26 g) in absolute ethanol (100 mL) was added **7** (19.7 mmol, 7.00 g) in absolute ethanol (100 mL). The reaction mixture was refluxed at 100 °C for 48 h. Ethanol was removed in vacuo, and the crude reddish-brown residue was purified by flash chromatography (1% MeOH/DCM) to give **5** (6.27 g, 72%) as a reddish-brown oil: R_f = 0.22 (1% MeOH/DCM); ^{1}H NMR (500 MHz, $CDCl_3$) δ 8.00 (s, 1H), 7.33 (d, *J* = 10 Hz, 2H), 7.22 (d, *J* = 10 Hz, 2H), 4.29 (q, *J* = 7.1 Hz, 2H), 4.13−4.01 (m, 2H), 3.14−3.05 (m, 1H), 3.03−2.94 (m, 1H), 2.66−2.51 (m, 2H), 2.31−2.20 (m, 2H), 1.50−1.30 (m, 2H), 1.43 (s, 9H), 1.35 (t, *J* = 7 Hz, 3H), 1.28 (d, *J* = 7 Hz, 6H); ^{13}C NMR (125 MHz, $CDCl_3$) δ 163.2, 154.7, 150.3, 149.6, 142.8, 137.0, 127.3, 126.3, 112.0, 79.3, 60.0, 47.2, 35.1, 33.8, 28.4, 27.2, 23.8, 14.3.

*5-(1-(tert-Butoxycarbonyl)piperidin-4-yl)-1-(4-isopropylphenyl)-1H-pyrazole-4-carboxylic acid (**9**).* To a stirred solution of **8** (14.2 mmol, 6.27 g) in 95% ethanol (35 mL) was added a 2.0 M NaOH solution (35 mL). The reaction mixture was refluxed at 70 °C for 20 h. Ethanol was removed in vacuo, and the resulting solid was acidified to pH 2 at 0 °C using 1 M HCl. The reddish-brown solid was filtered off and washed with cold water to give **9** (3.98 g, 68%): ^{1}H NMR (500 MHz, $CDCl_3$) δ 8.07 (s, 1H), 7.40−7.20 (m, 4H), 4.32−3.98 (m, 2H), 3.14 (app t, *J* = 12 Hz, 1H), 3.05−2.94 (m, 1H), 2.71−2.52 (m, 2H),

2.37−2.20 (m, 2H), 1.65−1.52 (m, 3H), 1.47 (s, 9H), 1.31 (d, J = 7 Hz, 6H); ^{13}C NMR (125 MHz, $CDCl_3$) δ 168.2, 154.8, 150.6, 150.4, 143.5, 136.8, 127.3, 126.3, 111.1, 79.5, 35.1, 33.8, 28.5, 28.4, 27.3, 23.8; HRMS calcd for $C_{23}H_{32}N_3O_4$ $(M + H)^+$ 414.2387, found 414.2385.

*tert-Butyl 4-(4-((3,5-Dimethylphenyl)carbamoyl)-1-(4-isopropylphenyl)-1H-pyrazol-5-yl)piperidine-1-carboxylate (**10**).* To a stirred solution of **9** (3.05 mmol, 1.26 g) and DMAP (0.30 mmol, 37 mg) in DCM (10 mL) at 0 °C were added DCC (3.35 mmol, 691 mg) and 3,5-dimethylaniline (3.35 mmol, 483 mg) sequentially. The reaction mixture was gradually warmed to rt and ran for 48 h. DCM was removed in vacuo, and the crude mixture was purified by flash chromatography (30% EA/Hex) to give **10** (745 mg, 47%) as a brownish solid: ^{1}H NMR (500 MHz, $CDCl_3$) δ 7.85 (s, 1H), 7.69 (s, 1H), 7.33 (d, J = 8.3 Hz, 2H), 7.24 (d, J = 8.3 Hz, 2H), 7.20 (s, 1H), 6.76 (s, 1H), 4.25−3.97 (m, 2H), 3.16 (app t, J = 12 Hz, 1H), 3.00 (app p, J = 7 Hz, 1H), 2.71−2.48 (m, 2H), 2.30 (s, 6H), 2.26−2.17 (m, 2H), 1.67−1.56 (m, 2H), 1.42 (s, 9H), 1.29 (d, J = 7 Hz, 6H); ^{13}C NMR (125 MHz, $CDCl_3$) δ 161.6, 154.8, 150.42, 148.9, 138.8, 138.5, 137.7, 137.2, 127.3, 126.5, 126.1, 117.9, 115.9, 79.3, 35.1, 33.9, 30.3, 29.4, 28.4, 23.9, 21.4; R_f = 0.33 (30% EA/Hex); MS calcd for $C_{31}H_{39}N_4O_3$ $(M - H)^-$ 515.3028, found 515.3030.

*N-(3,5-Dimethylphenyl)-1-(4-isopropylphenyl)-5-(piperidin-4-yl)-1H-pyrazole-4-carboxamide (**3**).* To a stirred solution of **10** (1.44 mmol, 745 mg) in DCM (5 mL) at 0 °C was added TFA (5 mL). The reaction mixture was warmed to rt and stirred for 1 h. The solvents were removed in vacuo. The organic residue was redissolved in DCM. The organic layer was washed with saturated sodium bicarbonate and then brine and dried over $MgSO_4$. The solvent was removed in vacuo to yield **3** (590 mg, 98%) as a brown solid: ^{1}H NMR (500 MHz, $CDCl_3$) δ 7.86 (s, 1H), 7.49 (s, 1H), 7.38 (d, J = 8.3 Hz, 2H), 7.25 (d, J = 8.3 Hz, 2H), 6.79 (s, 1H), 3.34−3.27 (m, 2H), 3.26−3.19 (m, 1H), 3.09−2.95 (m, 1H), 2.72 (app t, J = 13.2 Hz, 2H), 2.46 (qd, J = 13, 9.7, 3.7 Hz, 2H), 2.32 (s, 6H), 1.74 (d, J = 15 Hz, 2H), 1.32 (d, J = 7 Hz, 6H); ^{13}C NMR (125 MHz, $CDCl_3$) δ 161.8, 150.3, 149.1, 138.73, 138.69, 137.8, 137.0, 127.4, 126.2, 126.1, 118.0, 115.8, 46.2, 34.9, 33.9, 30.2, 23.8, 21.4; MS calcd for $C_{26}H_{33}N_4O$ $(M + H)^+$ 417.2649, found 417.2646.

*Diethyl 2-(Benzo[d][1,3]dioxol-5-ylmethylene)malonate (**11**).* To a solution of diethyl malonate (31.2 mmol, 5.0 g) and piperonal (37.4, 5.61 g) in toluene (80 mL) was added piperidine (3.12 mmol, 0.308 mL) followed by acetic acid (3.12 mmol, 0.179 mL). The reaction was refluxed at 150 °C under Dean−Stark conditions for 24 h. The reaction mixture was purified by flash chromatography (20% EA/Hex) to give an inseparable mixture of **8** and aldehyde (3.83 g, 42%) as a clear oil: TLC R_f = 0.31 (20% EA/Hex). ^{1}H NMR showed **11** constituted 86% of the mixture (3.29 g, 36%): ^{1}H NMR (500 MHz, $CDCl_3$) δ 7.61 (s, 1H), 7.01−6.98 (m, 1H), 6.96−6.94 (m, 1H), 6.82−6.78 (m, 1H), 6.00 (s, 2H), 4.36 (q, J = 7.1 Hz, 2H), 4.28 (q, J = 7.1 Hz, 2H), 1.32 (2t, J = 7.2 Hz, 6H); ^{13}C NMR (126 MHz, $CDCl_3$) δ 190.2, 166.9, 164.2, 149.8, 148.2, 141.6, 128.5, 126.9, 126.1, 124.0, 108.5, 108.3, 108.3, 106.8, 102.0, 101.6, 61.6, 61.4, 14.1, 13.8; HRMS calcd for $C_{15}H_{17}O_6$ $(M + H)^+$ 293.1020, found 293.1025.

*(±)-Diethyl 2-(1-(Benzo[d][1,3]dioxol-5-yl)-2-phenylethyl)malonate (**12**).* Under argon, **11** (9.61 mmol, 2.81 g) in dry Et_2O (30 mL) was added slowly via cannula to a suspension of CuCl (0.481 mmol, 48 mg) and benzyl magnesium chloride (11.5 mmol, 5.75 mL) at −78 °C. The mixture was stirred while the temperature was gradually raised to rt overnight. Saturated NH_4Cl was added. The aqueous layer was extracted with Et_2O (3×). The combined organic extracts were washed with brine and dried over $MgSO_4$. The crude residue was purified by flash chromatography (10% EA/Hex) to give **12** (2.26 g, 98%) as a yellowish oil. The product was directly used for the following step without further purification. MS: calcd for $C_{22}H_{25}O_6$ $(M + H)^+$ 385.1646, found 385.1654

*(±)-3-(Benzo[d][1,3]dioxol-5-yl)-4-phenylbutanoic Acid (**13**).* To a stirred solution of **12** (5.37 mmol, 2.06 g) in MeOH/H_2O (1:1, 40 mL) was added a 10% KOH solution (40 mL) in one portion. The reaction mixture was stirred at rt for 24 h. MeOH was removed in vacuo, and the water layer was acidified to pH 2 with 6 N HCl at 0 °C. The precipitate was collected by vacuum filtration. The crude solid was dissolved in *p*-xylene (30 mL) and refluxed overnight at 170 °C. The crude mixture was purified by flash chromatography (10% EA/Hex) to yield **13** (1.42 g, 93%) as a white solid: TLC R_f = 0.17 (10% EA/Hex); ^{1}H NMR (500 MHz, $CDCl_3$) δ 7.28−7.14 (m, 3H), 7.09−7.03 (m, 2H), 6.73−6.65 (m, 2H), 6.61−6.55 (m, 1H), 5.92 (s, 2H), 3.38−3.28 (m, 1H), 2.91−2.82 (m, 2H), 2.70−2.54 (m, 2H); ^{13}C NMR (125 MHz, $CDCl_3$) δ 177.1, 147.6, 146.2, 139.3, 137.0, 129.2, 128.3, 126.3, 120.6, 108.2, 107.7, 100.9, 43.4, 43.1, 39.9; MS calcd for $C_{17}H_{17}O_4$ $(M + H)^+$ 285.1121, found 285.1116.

*(±)-3-(Benzo[d][1,3]dioxol-5-yl)-4-phenylbutan-1-ol (**14**).* **13** (4.9 mmol, 1.39 g) in dry THF (50 mL) was added dropwise to a slurry of lithium aluminum hydride (9.8 mmol, 372 mg) in dry THF (30 mL) at 0 °C over 30 min. The reaction mixture was stirred and gradually warmed to rt over 4 h. The reaction mixture was cooled again to 0 °C, and water was added until evolution of gas ceased. The resultant slurry was filtered over Celite with washing with Et_2O. THF was removed in vacuo. The crude residue was purified by flash chromatography (30% EA/Hex) to yield **14** (1.14 g, 86%) as a clear oil: TLC R_f = 0.27 (30% EA/Hex); ^{1}H NMR (500 MHz, $CDCl_3$) δ 7.25−7.10 (m, 3H), 7.08−7.03 (m, 2H), 6.74−6.66 (m, 2H), 6.59−6.54 (m, 1H), 5.92 (s, 2H), 3.55−3.47 (m, 1H), 3.46−3.38 (m, 1H), 2.99−2.90 (m, 1H), 2.89−2.82 (m, 2H), 1.98−1.88 (m, 1H), 1.85−1.73 (m, 1H); ^{13}C NMR (125 MHz, $CDCl_3$) δ 147.6, 145.8, 140.2, 138.1, 129.1, 128.1, 125.9, 120.8, 108.0, 107.6, 100.7, 60.9, 44.1, 43.9, 38.3; MS calcd for $C_{17}H_{19}O_3$ $(M + H)^+$ 271.1329, found 271.1326.

*(±)-3-(Benzo[d][1,3]dioxol-5-yl)-4-phenylbutanal (**15**).* To a stirred solution of **14** (4.04 mmol, 1.09 g), triethylamine (20.2 mmol, 2.8 mL), and DMSO (109 mmol, 7.7 mL) in DCM (20 mL) at 0 °C was added SO_3·Py (20.2 mmol, 3.21 g) portionwise over 5 min. The reaction mixture was stirred for 2 h and subsequently warmed to rt. Excess sodium bicarbonate was then added and the mixture stirred until all remaining SO_3·Py was consumed. The organic solution was diluted with DCM, washed with brine, and dried over $MgSO_4$, and solvent was removed in vacuo. The crude residue was purified by flash chromatography (20% Et_2O/Hex) to give **15** (871 mg, 80%) as a yellowish oil: TLC R_f = 0.24 (20% Et_2O/Hex); ^{1}H NMR (500 MHz, $CDCl_3$) δ 9.59 (s, 1H), 7.29−7.15 (m, 3H), 7.09−7.03 (2H), 6.73−6.65 (m, 2H), 6.63−6.56 (m, 1H), 5.92 (s, 2H), 3.47−3.37 (m, 1H), 2.95−2.80 (m, 2H), 2.70 (d, J = 8.1 Hz, 2H); ^{13}C NMR (125 MHz, $CDCl_3$) δ 201.5, 147.8, 146.2, 139.2, 137.0, 129.1, 128.3, 126.3, 120.6, 108.2, 107.6, 100.9, 49.1, 43.4, 41.8; MS calcd for $C_{17}H_{15}O_3$ $(M - H)^-$ 267.1027, found 267.1030.

4-(((3-(Benzo[*d*][1,3]dioxol-5-yl)-4-phenylbutyl)amino)-methyl)-*N*,*N*-dimethylaniline (2). Under argon a flask was charged with **15** (36 mg, 0.13 mmol), THF (2 mL), and 4-(dimethylamino)benzylamine dihydrochloride (58 mg, 0.26 mmol). $Na(AcO)_3BH$ (55 mg, 0.26 mmol) was added with stirring at rt. After 20 h, 1 M NaOH (2 mL) was added. The mixture was extracted with Et_2O (3 × 10 mL). The extract was dried over $MgSO_4$ and solvent removed in vacuo. The crude material was purified by column chromatography (2%−5% (10% NH_4OH/MeOH)/DCM) to give **2** (13 mg, 25%) as a colorless oil: TLC R_f = 0.18 (5% (10% NH_4OH/MeOH/DCM); ^{1}H NMR (500 MHz, $CDCl_3$) δ 7.24−7.10 (m, 5H), 7.05−6.98 (m, 2H), 6.70−6.62 (m, 4H), 6.55−6.48 (m, 1H), 5.90 (d, J = 5 Hz, 2H), 3.69−3.52 (m, 2H), 2.91 (s, 6H), 2.82 (s, 3H), 2.53−2.45 (m, 2H), 2.00−1.77 (m, 2H); ^{13}C NMR (125 MHz, $CDCl_3$) δ 150.0, 147.5, 145.7, 140.1, 138.0, 129.5, 129.1, 128.0, 125.8, 120.8, 112.5, 108.0, 107.6, 100.7, 52.5, 46.4, 45.6, 43.9, 40.6, 34.8; MS calcd for $C_{26}H_{31}N_2O_2$ $(M + H)^+$ 403.2380, found 403.2385.

Pharmacokinetics of the Leads in Rodents. A method to quantify **3** in plasma was developed using HPLC−MS/MS (API 3200; Applied Biosystems). A 20 μL plasma sample was extracted with methyl tertiary butyl ether (MTBE) under neutral conditions (0.1 M phosphate buffer pH = 7.4) using temazepam as the internal standard. The extract is evaporated, reconstituted with mobile phase and injected into the HPLC. The HPLC column is a C-8 50 × 4.6 mm 5 μm column and separation of **3** and temazepam occurred by a linear gradient mobile phase starting with acetonitrile:0.1% formic acid (10:90) and changing to 80:20. The m/z Q1 and Q3 settings on the API 3200 for **3** and temazepam are 418/297 and 301/255, respectively. The lower limit of quantification of **3** is 1 ng/mL using 20 μL of plasma. A standard response curve of **3** was created with concentrations that varied from 1 ng/mL to 1000 ng/mL using 300 ng/mL of temazepam for each sample.

In order to determine drug concentrations of the lead inhibitors in the pharmacological models, we first need to characterize the PK properties of the compounds in mice. The PK of **3** was determined in NOD/SCID mice following a single dose given po. The study design used 3 mice per time point. Blood was collected at time intervals from 0 to 24 h after dosing (8 time points), quantified by the procedure described above. Pharmacokinetic parameters for **3** including area under the curve (AUC), area under the moment curve (AUMC), and $t_{1/2}$ were estimated using noncompartmental methods with Excel. The maximum plasma concentration (C_{max}) and time of C_{max} (t_{max}) were obtained from the data. The AUC from zero to infinity ($AUC_{0-\infty}$) was estimated from the AUC_{0-t} (time zero to the last quantifiable concentration C_{last}) and the AUC from C_{last} to infinity, C_{last}/k_{el}, where k_{el} is the rate constant of elimination. The $AUMC_{0-\infty}$ was estimated by an analogous manner. The systemic clearance (Cl/F, where F = bioavailability) of **3** was calculated from the dose and $AUC_{0-\infty}$.

Mouse Xenograft Studies. NOD/SCID mice were obtained from the on-site breeding colony maintained by the In Vivo Therapeutics Core at the Indiana University Simon Cancer Center (IUSM, Indianapolis, IN) and maintained in pathogen-free conditions within the laboratory animal resources center (LARC) at the Indiana University School of Medicine according to an approved protocol by the Institutional Animal Care and Use Committee (IACUC) committee. TMD-231 cells (1×10^6) were injected into the mammary fat pads (mfp) of 4−6 week old mice. These cells have been shown previously to develop primary tumors and metastasize efficiently to the lungs when the primary tumors have been removed.[37] For metastasis studies, mfp tumors were allowed to grow to ~100 mm^3 in mice. Mice were assigned to a treatment group based on average tumor size/weight. Following a recovery period of two days, mice received treatment of investigational drug (n = 15) or a PBS solvent control (n = 15). After four weeks mice were euthanized, and the lungs were resected, fixed in formalin solution, sectioned, and stained with hematoxylin and eosin (H&E) for analysis. The number and size of metastasis in two to five fields per sample were calculated, a score of 4+ was given to the sample with the highest metastasis index, and relative metastasis in other samples was calculated (i.e., 1+, 2+, 3+) by a sample-blinded pathologist. Tumor volume was calculated as length × $width^2/2$ in millimeters.

AUTHOR INFORMATION

Corresponding Author

*Tel: (317) 274-8315. Fax: (317) 278-9217. E-mail: smeroueh@iupui.edu.

Author Contributions

‡These authors contributed equally.

ACKNOWLEDGMENT

The research was supported by the National Institutes of Health (CA135380) (S.O.M.), an INGEN grant from the Lilly Endowment, Inc. (S.O.M.), the Indiana University Melvin and Bren Simon Cancer Center Translational Research Acceleration Collaboration (ITRAC) (S.O.M.), the Showalter Trust (S.O.M.), the Indiana University Biomedical Research Fund (S.O.M.) and an American Cancer Society Institutional Grant (S.O.M.). Computer time on the Big Red supercomputer at Indiana University is funded by the National Science Foundation and by Shared University Research grants from IBM, Inc., to Indiana University. We are thankful to the TeraGrid for computer time. We thank Dr. Khalil Bdeir for providing stable cell lines for expression of uPAR in *Drosophila* S2 cells. We acknowledge the Angiogenesis, Endothelial & Pro-Angiogenic Cell Core (AEPCC) of the Indiana University Simon Cancer Center for performing the matrigel tube formation assays, and the analytical work performed by the Clinical Pharmacology Analytical Core laboratory, a core laboratory of the Indiana University Melvin and Bren Simon Cancer Center supported by National Cancer Institute Grant P30 CA082709. We thank Dr. Jed Fisher for his careful reading of the manuscript and suggestions.

ABBREVIATIONS USED

uPAR, urokinase receptor; uPA, urokinase-type plasminogen activator; suPAR, soluble urokinase receptor; MMP, matrix metalloproteinase; RTK, receptor tyrosine kinase; GPCR, G-protein coupled receptor; ECM, extracellular matrix; GFD, growth factor-like domain; HUVEC, human umbilical vein endothelial cells; MAPK, mitogen-activated protein kinase; FAK, focal adhesion kinase; DMSO, dimethyl sulfoxide; hERG, human ether-à-go-go related gene; FP, fluorescence polarization; CYP, cytochrome P450; FDA, food and drug administration; EB, ethidium bromide; DNA, DNA; NOD/SCID, non-obese diabetic severe combined immunodeficient; PK, pharmacokinetic; PBS, phosphate buffered saline; Src, sarcoma; MDA-MB-231, MD Anderson metastatic breast; FBS, fetal bovine serum; DMEM, Dulbecco's modified Eagle medium; SDS, sodium dodecyl sulfate; CBB, Coomassie brilliant blue; BSA, bovine serum albumin; DEAE, diethylaminoethyl cellulose; FITC, fluorescein isothiocyanate; TBST, Tris-buffered saline and Tween 20; IB, immunoblot; NMR, nuclear magnetic resonance; DCM, dichloromethane; HRMS, high-resolution mass spectrometry; THF, tetrahydrofuran; PDB, protein databank; DMAP, 4-dimethylaminopyridine; DCC, *N*,*N*′-dicyclohexylcarbodiimide; FAM, 6-carboxyfluorescein; HPLC, high-performance liquid chromatography; GPI, glycosylphosphatidylinositol; MTT, 3-(4,5-dimethylthiazol-2-yl)-2,5-diphenyltetrazolium bromide; TMD-231, tumor-derived 231; AUC, area under the curve; AUMC, area under the moment curve; LARC, laboratory animal resources center; IACUC, Institutional Animal Care and Use Committee; HPLC, high-performance liquid chromatography; FN, fibronectin; ActD, actinomycin D.

REFERENCES

(1) Sporn, M. B. The war on cancer. *Lancet* **1996**, *347*, 1377–1381.

(2) Wei, Y.; Lukashev, M.; Simon, D. I.; Bodary, S. C.; Rosenberg, S.; Doyle, M. V.; Chapman, H. A. Regulation of integrin function by the urokinase receptor. *Science* **1996**, *273*, 1551–1555.

(3) Kiyan, J.; Kiyan, R.; Haller, H.; Dumler, I. Urokinase-induced signaling in human vascular smooth muscle cells is mediated by PDGFR-beta. *EMBO J.* **2005**, *24*, 1787–1797.

(4) Liu, D.; Aguirre Ghiso, J.; Estrada, Y.; Ossowski, L. EGFR is a transducer of the urokinase receptor initiated signal that is required for in vivo growth of a human carcinoma. *Cancer Cell* **2002**, *1*, 445–457.

(5) Shapiro, R. L.; Duquette, J. G.; Nunes, I.; Roses, D. F.; Harris, M. N.; Wilson, E. L.; Rifkin, D. B. Urokinase-type plasminogen activator-deficient mice are predisposed to staphylococcal botryomycosis, pleuritis, and effacement of lymphoid follicles. *Am. J. Pathol.* **1997**, *150*, 359–369.

(6) Kirchheimer, J. C.; Wojta, J.; Christ, G.; Binder, B. R. Proliferation of a human epidermal tumor cell line stimulated by urokinase. *FASEB J.* **1987**, *1*, 125–128.

(7) Kirchheimer, J. C.; Wojta, J.; Christ, G.; Binder, B. R. Functional inhibition of endogenously produced urokinase decreases cell proliferation in a human melanoma cell line. *Proc. Natl. Acad. Sci. U.S.A.* **1989**, *86*, 5424–5428.

(8) Andreasen, P. A.; Kjoller, L.; Christensen, L.; Duffy, M. J. The urokinase-type plasminogen activator system in cancer metastasis: A review. *Int. J. Cancer* **1997**, *72*, 1–22.

(9) Mignatti, P.; Rifkin, D. B. Plasminogen activators and matrix metalloproteinases in angiogenesis. *Enzyme Protein* **1996**, *49*, 117–137.

(10) Rabbani, S. A.; Mazar, A. P. The role of the plasminogen activation system in angiogenesis and metastasis. *Surg. Oncol. Clin. N. Am.* **2001**, *10*, 393–415.

(11) Kim, J.; Yu, W.; Kovalski, K.; Ossowski, L. Requirement for specific proteases in cancer cell intravasation as revealed by a novel semiquantitative PCR-based assay. *Cell* **1998**, *94*, 353–362.

(12) Eldridge, M. D.; Murray, C. W.; Auton, T. R.; Paolini, G. V.; Mee, R. P. Empirical scoring functions: I. The development of a fast empirical scoring function to estimate the binding affinity of ligands in receptor complexes. *J. Comput.-Aid. Mol. Des.* **1997**, *11*, 425–445.

(13) Jones, G.; Willett, P.; Glen, R. C.; Leach, A. R.; Taylor, R. Development and validation of a genetic algorithm for flexible docking. *J. Mol. Biol.* **1997**, *267*, 727–748.

(14) Huey, R.; Morris, G. M.; Olson, A. J.; Goodsell, D. S. A semiempirical free energy force field with charge-based desolvation. *J. Comput. Chem.* **2007**, *28*, 1145–1152.

(15) Huang, N.; Kalyanaraman, C.; Irwin, J. J.; Jacobson, M. P. Physics-based scoring of protein-ligand complexes: enrichment of known inhibitors in large-scale virtual screening. *J. Chem. Inf. Model.* **2006**, *46*, 243–253.

(16) Huai, Q.; Zhou, A.; Lin, L.; Mazar, A. P.; Parry, G. C.; Callahan, J.; Shaw, D. E.; Furie, B.; Furie, B. C.; Huang, M. Crystal structures of two human vitronectin, urokinase and urokinase receptor complexes. *Nat. Struct. Mol. Biol.* **2008**, *15*, 422–423.

(17) Chen, H. C. Boyden chamber assay. *Methods Mol. Biol.* **2005**, *294*, 15–22.

(18) Ronne, E.; Behrendt, N.; Ploug, M.; Nielsen, H. J.; Wollisch, E.; Weidle, U.; Dano, K.; Hoyer-Hansen, G. Quantitation of the receptor for urokinase plasminogen activator by enzyme-linked immunosorbent assay. *J. Immunol. Methods* **1994**, *167*, 91–101.

(19) Simon, D. I.; Wei, Y.; Zhang, L.; Rao, N. K.; Xu, H.; Chen, Z. P.; Liu, Q. M.; Rosenberg, S.; Chapman, H. A. Identification of a urokinase receptor-integrin interaction site - Promiscuous regulator of integrin function. *J. Biol. Chem.* **2000**, *275*, 10228–10234.

(20) Wei, Y.; Eble, J. A.; Wang, Z. M.; Kreidberg, J. A.; Chapman, H. A. Urokinase receptors promote beta 1 integrin function through interactions with integrin alpha 3 beta 1. *Mol. Biol. Cell* **2001**, *12*, 2975–2986.

(21) Wei, Y.; Tang, C. H.; Kim, Y.; Robillard, L.; Zhang, F.; Kugler, M. C.; Chapman, H. A. Urokinase receptors are required for alpha 5 beta 1 integrin-mediated signaling in tumor cells. *J. Biol. Chem.* **2007**, *282*, 3929–3939.

(22) Folkman, J. Angiogenesis in Cancer, Vascular, Rheumatoid and Other Disease. *Nat. Med.* **1995**, *1*, 27–31.

(23) Brown, S.; Meroueh, S. O.; Fridman, R.; Mobashery, S. Quest for selectivity in inhibition of matrix metalloproteinases. *Curr. Top. Med. Chem.* **2004**, *4*, 1227–1238.

(24) Wang, A. X.; Xie, Q.; Lane, B.; Mollison, K. W.; Hsieh, G. C.; Marsh, K.; Sheets, M. P.; Luly, J. R.; Coghlan, M. J. Synthesis and immunosuppressant activity of pyrazole carboxamides. *Bioorg. Med. Chem. Lett.* **1998**, *8*, 2787–2792.

(25) Bashford, K. E.; Burton, M. B.; Cameron, S.; Cooper, A. L.; Hogg, R. D.; Kane, P. D.; MacManus, D. A.; Matrunola, C. A.; Moody, C. J.; Robertson, A. A. B.; Warne, M. R. The Bohlmann-Rahtz route to functionalised pyridine scaffolds and their use in library synthesis. *Tetrahedron Lett.* **2003**, *44*, 1627–1629.

(26) Clay, R. J.; Collom, T. A.; Karrick, G. L.; Wemple, J. A Safe, Economical Method for the Preparation of Beta-Oxo Esters. *Synthesis* **1993**, 290–292.

(27) Plesner, T.; Ploug, M.; Ellis, V.; Ronne, E.; Hoyer-Hansen, G.; Wittrup, M.; Pedersen, T. L.; Tscherning, T.; Dano, K.; Hansen, N. E. The receptor for urokinase-type plasminogen activator and urokinase is translocated from two distinct intracellular compartments to the plasma membrane on stimulation of human neutrophils. *Blood* **1994**, *83*, 808–815.

(28) Shoemaker, A. R.; Oleksijew, A.; Bauch, J.; Belli, B. A.; Borre, T.; Bruncko, M.; Deckwirth, T.; Frost, D. J.; Jarvis, K.; Joseph, M. K.; Marsh, K.; McClellan, W.; Nellans, H.; Ng, S.; Nimmer, P.; O'Connor, J. M.; Oltersdorf, T.; Qing, W.; Shen, W.; Stavropoulos, J.; Tahir, S. K.; Wang, B.; Warner, R.; Zhang, H.; Fesik, S. W.; Rosenberg, S. H.; Elmore, S. W. A small-molecule inhibitor of Bcl-XL potentiates the activity of cytotoxic drugs in vitro and in vivo. *Cancer Res.* **2006**, *66*, 8731–8739.

(29) Guengerich, F. P. Common and uncommon cytochrome P450 reactions related to metabolism and chemical toxicity. *Chem. Res. Toxicol.* **2001**, *14*, 611–650.

(30) Huang, Q.; Petros, A. M.; Virgin, H. W.; Fesik, S. W.; Olejniczak, E. T. Solution structure of the BHRF1 protein from Epstein-Barr virus, a homolog of human Bcl-2. *J. Mol. Biol.* **2003**, *332*, 1123–1130.

(31) Li, L.; Li, J.; Khanna, M.; Jo, I.; Baird, J. P.; Meroueh, S. O. Docking to erlotinib off-targets leads to inhibitors of lung cancer cell proliferation with suitable pharmacokinetics. *ACS Med. Chem. Lett.* **2010**, *1*, 229–233.

(32) Kelekar, A.; Chang, B. S.; Harlan, J. E.; Fesik, S. W.; Thompson, C. B. Bad is a BH3 domain-containing protein that forms an inactivating dimer with Bcl-XL. *Mol. Cell. Biol.* **1997**, *17*, 7040–7046.

(33) Zhong, S.; Chen, X.; Zhu, X.; Dziegielewska, B.; Bachman, K. E.; Ellenberger, T.; Ballin, J. D.; Wilson, G. M.; Tomkinson, A. E.; MacKerell, A. D. Identification and validation of human DNA ligase inhibitors using computer-aided drug design. *J. Med. Chem.* **2008**, *51*, 4553–4562.

(34) Dorfleutner, A.; Stehlik, C.; Zhang, J.; Gallick, G. E.; Flynn, D. C. AFAP-110 is required for actin stress fiber formation and cell adhesion in MDA-MB-231 breast cancer cells. *J. Cell Physiol.* **2007**, *213*, 740–749.

(35) Chavakis, T.; Kanse, S. M.; Lupu, F.; Hammes, H. P.; Muller-Esterl, W.; Pixley, R. A.; Colman, R. W.; Preissner, K. T. Different mechanisms define the antiadhesive function of high molecular weight kininogen in integrin- and urokinase receptor-dependent interactions. *Blood* **2000**, *96*, 514–522.

(36) Jibrini, M. B.; Molnar, J.; Arora, R. R. Prevention of atrial fibrillation by way of abrogation of the renin-angiotensin system: a systematic review and meta-analysis. *Am. J. Ther.* **2008**, *15*, 36–43.

(37) Hochreiter, A. E.; Xiao, H.; Goldblatt, E. M.; Gryaznov, S. M.; Miller, K. D.; Badve, S.; Sledge, G. W.; Herbert, B. S. Telomerase template antagonist GRN163L disrupts telomere maintenance, tumor growth, and metastasis of breast cancer. *Clin. Cancer Res.* **2006**, *12*, 3184–3192.